Band structure of segmented semiconductor nanowires

M.-E. Pistol*
Division of Solid State Physics/The Nanometer Structure Consortium, Lund University, P.O. Box 118, S-221 00 Lund, Sweden

C. E. Pryor†
Department of Physics and Astronomy and Optical Science and Technology Center, University of Iowa, Iowa City, Iowa 52242, USA
(Received 8 March 2009; revised manuscript received 12 June 2009; published 23 July 2009)

We have calculated the band structures for strained segmented nanowires involving all combinations of AlN, GaN, InN, AlP, GaP, AlAs, GaAs, InP, InAs, AlSb, GaSb, and InSb, as a function of segment length. This was done for two different growth directions of the wires, [100] and [111]. Both the Γ and the X conduction-band minima were included in the calculations as well as the valence bands. Short segments behave like strained quantum wells and our results thus include strained quantum wells as a subset. We find all material combinations that give metallic segments due to a negative band gap and we find all the band alignments that may occur. We identify those structures which show spontaneous charge separation as well as those which are suitable for the optical generation of polarized exciton gases, with their rich phase diagram, theoretically predicted to include superfluids and supersolids. Some device related ideas are presented. Due to the amount of data (several hundreds of diagrams) most of our results are presented as a webpage.

DOI: 10.1103/PhysRevB.80.035316 PACS number(s): 73.22.−f, 73.21.Hb

I. INTRODUCTION

Nanowires made from semiconductors are highly versatile structures.[1] They can be made from a wide variety of materials and they can contain segments of different materials, that is, heterostructures can easily be made.[2] It is also possible to fabricate core-shell heterostructures by capping a seed wire with a suitable shell material.[3,4] The two techniques can also be combined, allowing the fabrication of quantum dots within the nanowires. Nanowires are often fabricated by using a metal particle as a catalyst and the wire grows below the metal particle. It is thus possible to position the wires in predefined positions if the metal particles are fabricated by lithography. One cm^2 can be made to contain 10^{11} wires—allowing highly parallel operations. The wires have applications in biology and optics and are expected to have interesting transport properties[5,6] due to their predicted low phonon scattering rate.[7] There is a large set of materials that can be combined in heterostructure wires and it is highly useful if theory can guide the fabrication of interesting structures and this problem is addressed in this paper. There have been several theoretical methods applied to calculate the electronic structure of nanowires; for a review see Ref. 8. Most theoretical work on heterostructured wires have focused on one specific materials combination, although for core-shell wires many materials combinations have been studied.[9]

We have calculated the band structure of segmented wires as a function of segment length. All combinations of AlN, GaN, InN, AlP, GaP, AlAs, GaAs, InP, InAs, AlSb, GaSb, and InSb, where one compound is a segment in another, were calculated. Two geometries of the wires were considered: wires having a hexagonal cross section oriented along the [111] direction and wires having a square cross section oriented along the [100] direction. These are the two most common geometries found in experiments[10] and are illustrated in Fig. 1. The crystal structure of the compounds was assumed to be that of zinc blende. In our calculations we have included the X band minima, the Γ band minimum and the valence bands, including the spin-orbit split off band. The amount of data is too large to include in a paper, so we have published a webpage that contains all the computed band structures.[11] We have also published tables of the band edge energies in the supplementary material for this paper.[12] Here we will illustrate the strain situation in segmented wires as well as give examples of some of the more interesting structures that can be made. These include wires which have segments with a negative band gap (i.e., metallic), wires with spontaneous charge polarization, and wires in which adjacent electron and hole gases can be created optically. We also highlight the combinations with unusually small band gaps or unusually large band gaps. A table summarizing the expected band alignments for all the combinations is given allowing an overview of all possibilities that can be realized. Since short segments are effectively two-dimensional strained layers, our results include this case as illustrated in three overview figures.

II. METHOD

The band structures were determined by first calculating the strain on a grid of $120\times120\times120$ points, which was

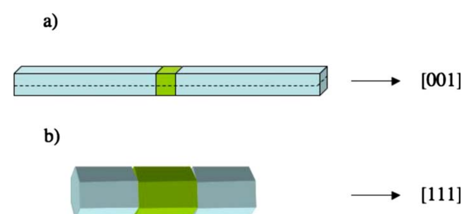

FIG. 1. (Color online) (a) A drawing of a segmented wire with a square cross section, oriented along the [001] direction, in this paper being defined as the z direction. The dashed line indicates the yz plane in which was used for the calculations shown in Figs. 2, 3, 5, and 6. (b) A drawing of a segmented wire having a hexagonal cross section, oriented along the [111] direction.

 ©2009 The American Physical Society

TABLE I. Deformation potentials used for the X conduction-band minimum. The values were taken from Refs. 13 and 14.

	Segment material											
Barrier material	AlN	GaN	InN	AlP	GaP	AlAs	GaAs	InP	InAs	AlSb	GaSb	InSb
Ξ_u	6.6	7.1	7.0	6.75	6.5	5.1	6.5	3.3	3.7	5.4	6.46	4.53
Ξ_d	−7.5	−3.11	−3.13	2.72	1.13	2.77	1.0	1.7	1.36	1.8	0.67	1.41

then used to compute energies at points within the structure using strain-dependent $\mathbf{k}\cdot\mathbf{p}$ theory. The strain was numerically calculated using continuum elasticity by taking a cubic grid in which each cube corresponds to a material of the structure. For a zinc-blende material the elastic energy of such a cube is given by[15]

$$F = \int \frac{1}{2}C_{11}(e_{xx}^2 + e_{yy}^2 + e_{zz}^2) + C_{12}(e_{xx}e_{yy} + e_{xx}e_{zz} + e_{yy}e_{zz}) + 2C_{44}(e_{xy}^2 + e_{xz}^2 + e_{yz}^2) - \alpha(e_{xx} + e_{yy} + e_{zz})d^3x, \tag{1}$$

where the C's are material-dependent elastic constants, α is a parameter used to implement the lattice mismatch, and $e_{ij} = \frac{1}{2}(\partial_i u_j + \partial_j u_i)$ is the strain tensor where u_i is the displacement. The displacement is defined on grid sites and linearly interpolated within each cube so the energy may be integrated to give F as a function of the displacements.

The lattice mismatch is implemented by taking one material (with lattice constant a_R) as a reference. For each cube we set $\alpha = (C_{11} + 2C_{12})(a_L - a_R)/a_R$ where a_L is the lattice constant of the material for that cube. With this value of α an isolated cube would relax so that the length of each edge changed by a factor $(a_L - a_R)/a_R$ reflecting its different lattice constant relative to the reference material. Under such a relaxation the strain of the cube would be $e_{ij}^0 = \delta_{ij}(a_L - a_R)/a_R$, which is a fictitious strain from straining the coordinate system. The physical strain is found by minimizing the total elastic energy using the conjugate gradient algorithm and then taking $e_{ij} - e_{ij}^0$ for each cube. While this method works for any grid spacing, the case in which the grid spacing is set to the crystal lattice constant is appealing because each cubic block is a unit cell. Because the minimum of the strain is scale invariant (i.e., invariant under $x \to ax$) the calculated strain field applies to any structure of the same shape that may be obtained by rescaling.

The zone-center energies were found by computing the eigenvalues of the $\mathbf{k}=0$ strain-dependent $\mathbf{k}\cdot\mathbf{p}$ Hamiltonian (from Ref. 16) as a function of the spatially dependent strain field. The energy of the conduction-band minimum at the X point was calculated in the single band approximation using

$$E_X = \Xi_d \,\mathrm{Tr}\, e + \Xi_u k_i e_{ij} k_j, \tag{2}$$

where Ξ_d and Ξ_u are the deformation potentials, e_{ij} is the strain tensor, and k_i is a unit vector in the direction of the particular X valley being considered. The materials parameters were taken from Refs. 17 and 18 except for the X-valley deformation potentials, which were taken from other sources and are given in Table I. We assumed a temperature of 0 K. We have not calculated the L-band energies since the deformation potentials are not generally available. However, with the possible exception of GaSb,[19] we do not expect the L band to be the conduction-band minimum for any material combination and segment length.

Although the wurtzite crystal structure is commonly seen in nanowires,[1] we have assumed zinc-blende structures since material parameters are not generally available for the wurtzite forms. The band energies and elastic constants of those few wurtzite materials that have been measured are close to the corresponding zinc-blende materials, so we expect our results to be useful for wires having the wurtzite structure as well.

III. STRAIN

In this section we consider segmented wires in which the segment is under compression followed by wires in which the segment is under tension. The general behavior of the strain is very similar for all wires with a segment in compression (or a segment in tension) since the elastic compliances of the III-V semiconductors are quite similar. The magnitude of the strain effects depend on the lattice mismatch of course, but this gives only quantitative changes. The general influence of the strain on the conduction-band and the valence-band edges will also be illustrated. Here we encounter a second important parameter, the valence band offset which is not very sensitive to strain but affects the overall band structure. At the end of the section we will show that the differences between segmented wires grown along the [001] direction and the [111] direction occur mainly in the X conduction-band minima.

A. Segments in compression

We have chosen to illustrate the case of segments in compression with an InAs segment in InP, which is a popular choice for experiments. In Fig. 2 we show plots of the hydrostatic pressure, $\mathrm{Tr}\, e = e_{xx} + e_{yy} + e_{zz}$, in such a wire. The wire is in this case elongated along the [100] direction and has a square cross section. Since InAs has a larger lattice constant than InP we expect positive hydrostatic pressure in the segment (which corresponds to $\mathrm{Tr}\, e < 0$) and this is borne out in the calculations. The compression in the segment occurs immediately at the interface and is largest at the center of the segment. For longer segments the compression in the center becomes zero. In InP we observe, as expected, negative hydrostatic pressure and the pressure decreases on a similar length scale as the segment thickness. Somewhat counterintuitively we find that there is also a region of positive hydrostatic pressure in the InP. This region is located

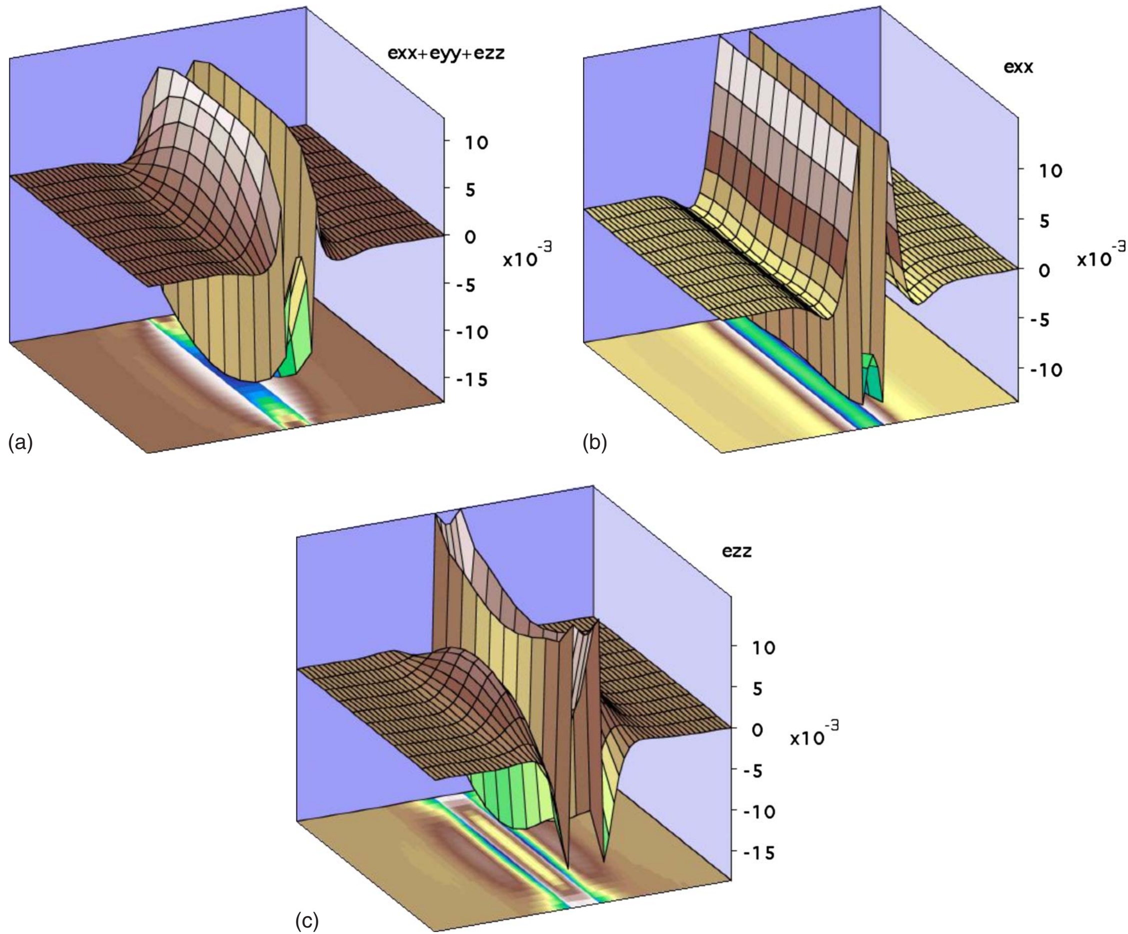

FIG. 2. (Color online) (a) A surface plot of $e_{xx}+e_{yy}+e_{zz}$ in a [001] oriented wire in the yz plane indicated in Fig. 1(a) consisting of an InAs segment in InP. The length of the InAs segment is 50 and the width of the wire is 100. The InAs segment is under hydrostatic pressure which is largest at the center of the segment and smallest at the surface of the segment. The InP is under tension close to the segment but is under weak compression further out before equilibrium is established. (b) A surface plot of e_{xx} in the wire. This strain tensor component has only weak variation across the wire. (c) A surface plot of e_{zz} in the wire. The behavior is quite complex and very different from that of e_{xx}.

outside the region of negative hydrostatic pressure.

The Γ conduction-band minima of the III-V semiconductors considered here are affected by the hydrostatic pressure alone and will be discussed below. The X conduction-band edges and the valence bands are also affected by the shear strain tensor elements, e_{xy}, e_{yz}, and e_{zx} as well as by inequalities among the diagonal elements. For a segment of InAs in InP, e_{xx} and e_{zz} behave very differently (Fig. 2). e_{xx} has a strong variation along the z direction but very small dependence on y. e_{xx} switches sign in the InP, being positive close to the interface and negative further out. The behavior of e_{zz} is very different, being more complex and depending on both y and z. In Fig. 3 we have plotted the conduction-band minimum and the valence-band maximum. The conduction-band minimum is at the surface of the InAs segment and is close to the bulk value. Electrons will be located there for wires sufficiently large that confinement can be neglected. In the valence band the situation is the same: the holes will have their lowest energy at the surface of the InAs segment where the band edge energy is close to the bulk value. This may be significant for optical recombination of excitons which is negatively affected by surface states.

In Fig. 4 we show line traces of all the bands that we have calculated. It can be seen that the strain effects are largest for short segments, which behave as a strained quantum well. For short segments we find that the X band minima are split, as is the valence-band maximum, which is a well known result for strained quantum wells. At a segment length of about 100 (where the wire width is 100) we observe that the situation in the center of the segment is bulklike and only at the interfaces do we observe strain affecting the band edges. The splitting of the X band minima and the valence-band maximum is small and this is also true at the interfaces.

B. Segments in tension

If the segment is under tension, (i.e., it has a smaller lattice constant than the rest of the wire), the situation is nearly the inverse of a wire with a segment in compression. The details depend or course on the values of the elastic compliances, which however are fairly similar among the III-V semiconductors. We illustrate the situation with an InAs wire containing an InP segment. The wire has a square cross section and is oriented along the [001] direction. The segment

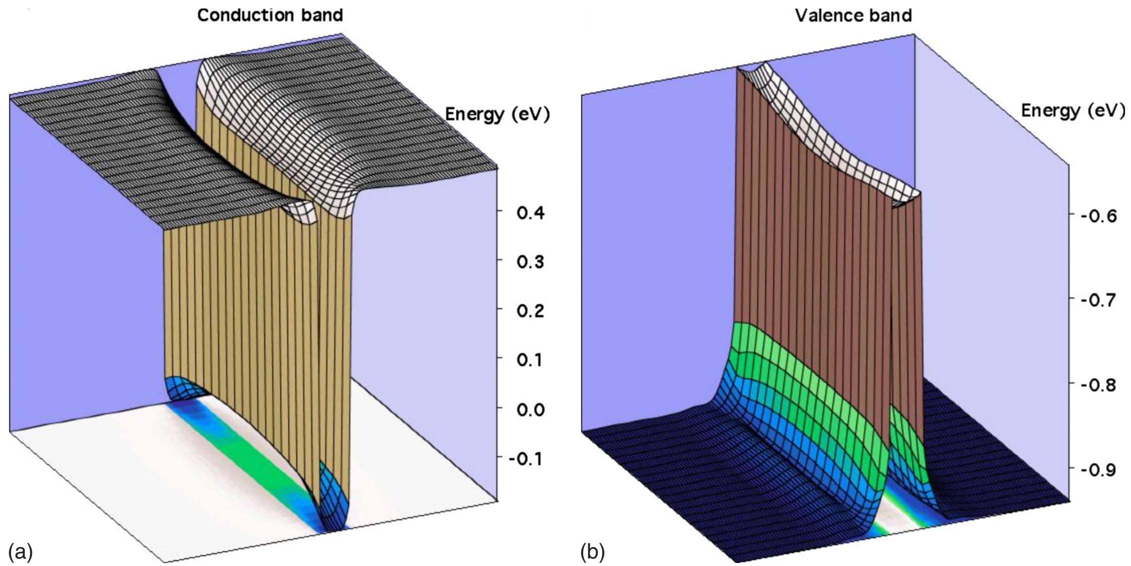

FIG. 3. (Color online) (a) A surface plot of the conduction-band minimum for a [001] oriented wire in the yz plane defined in Fig. 1(a), consisting of an InP wire with an InAs segment. The length of the InAs segment is 50 and the width of the wire is 100. (b) A surface plot of the valence-band maximum for the same wire.

length is 50 and the wire width is 100. Figure 5 shows the hydrostatic pressure, as well as e_{xx} and e_{zz} as a function of position in the wire within the plane shown in Fig. 1(a). We find that the tension is largest in the center of the segment and decreases toward its surface. In the InAs the hydrostatic pressure can be both compressive (as expected) as well as slightly tensional close to the surface of the wire. e_{xx} has only a weak dependence on y, but varies strongly with respect to z. e_{zz} has a more complicated behavior and depends strongly on both y and z. Figure 6 shows the conduction-band minimum and the valence-band maximum as a function of position. Since InP has a larger band gap than InAs the segment forms a barrier. The conduction-band barrier is highest at the surface of the wire. This could be an advantage for tunneling devices since the tunneling will take place in the center of the wire, away from the possibly deleterious effects of the surface. In the valence band we find that the barrier is quite flat in the transverse direction. We also see that there is a weak quantum well formed close to the segment within the InAs layer.

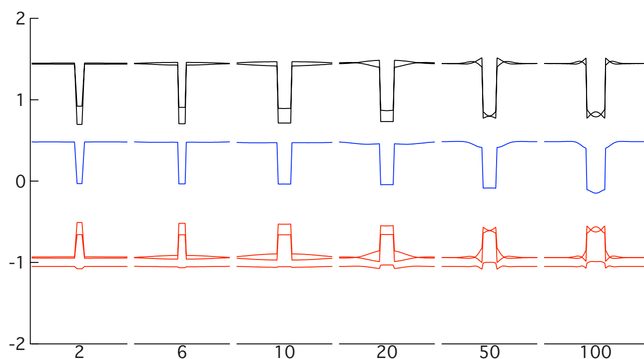

FIG. 4. (Color online) The band edges in an InAs/InP wire plotted along the [001] direction and through the center of the wire. The wire is the same as in Fig. 3. The length of the InAs segment was varied from 2 to 100, where the width of the wire (along the x direction) was 100. The blue trace is the Γ conduction band, black traces are the X conduction bands, and red traces are the valence bands.

In Fig. 7 we show line traces of the Γ conduction band, the X conduction band and the valence bands, at $\boldsymbol{k}=0$, for different segment lengths. A segment of length 2 behaves almost like a strained layer, similarly to the case where the segment was in compression. Also in a similar vein, a segment of length 100 behaves like bulk InP at its center. The Γ conduction band does not change very much with segment thickness. The X band is split when the segment is thin but for longer segments the splitting only persists at the interfaces. In the valence band we observe a quite strong splitting between the heavy and light holes for thin segments which becomes small for longer segments. The value of the valence-band barrier changes by several hundred meV depending on the segment length illustrating the importance of this parameter.

In Fig. 8 we show the conduction and valence bands of an InAs/InP junction in a heterostructure wire oriented along the [001] direction, which can be viewed as an infinitely long segment of InAs in InP. The behavior of the conduction band is fairly smooth and approaches the bulk value in a distance which is less than the wire width. In the valence band there is a shallow quantum well close to the interface on the "compressive side," i.e., in the InAs. No such well exists in the InP.

C. Wires oriented along the [111] direction

Nanowires are not limited to growth along the [001] direction but may also be grown with [111] orientation. It is thus important to know how the crystallographic orientation of the wire affects the band structure. Figure 9 shows line traces of the conduction bands and the valence bands for an

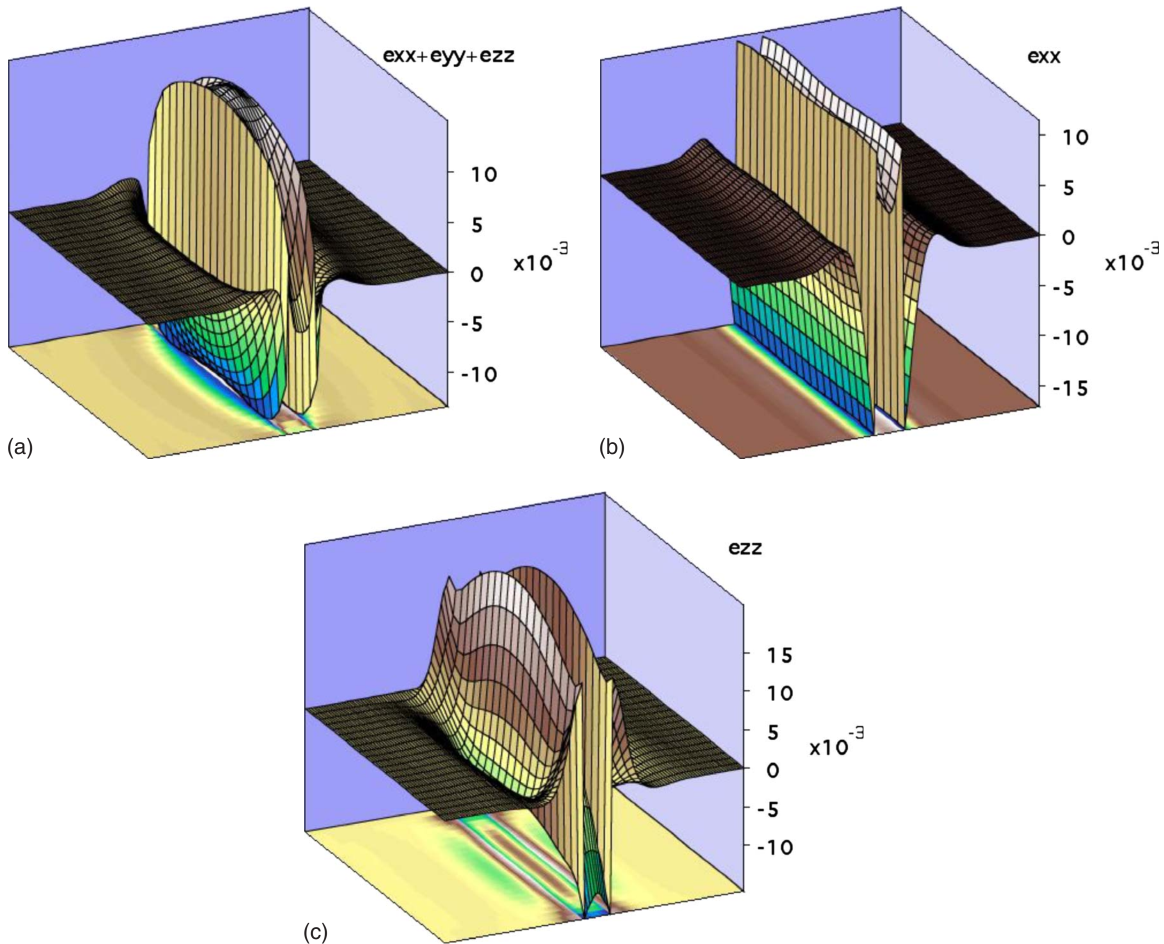

FIG. 5. (Color online) (a) A surface plot of $e_{xx}+e_{yy}+e_{zz}$ in a [001] oriented wire in the plane indicated in Fig. 1(a), consisting of an InAs wire with an InP segment. The length of the InP segment is 50 and the width of the wire is 100. The InP segment is under hydrostatic tension which is largest at the center of the segment and smallest at the surface of the segment. The InAs is under compression close to the segment and then is under weak tension further out before equilibrium is established. (b) A surface plot of e_{xx} in the wire. This strain tensor component has only a weak variation across the wire. (c) A surface plot of e_{zz} in the wire. The behavior is quite complex and very different from that of e_{xx}.

InP wire with an InAs segment, oriented along the [111] direction and having the hexagonal cross section illustrated in Fig. 1(b). The symmetry assures there is no splitting of the *X* band minima in the center of the wire. Apart from this we find the band structure to be very similar to that of wires oriented along the [001] direction shown in Fig. 4. The on-line results include both wire orientations, since for some orientations and material combinations the conduction-band minimum is at the *X* point.

IV. BAND STRUCTURES

In this section we comment on different materials combinations and point out some interesting structures, concentrating on the band alignment. In Fig. 10 we illustrate the different band alignments that are possible at the interface between two semiconductors. Tables II–IV summarize the different band alignments that may occur in the wire systems we have calculated and also gives the character of the smallest band gap: direct or indirect. Some materials combinations give interesting structures with a negative band gap which are thus metallic. We have not included nitrides on non-nitrides in the tables since they usually cannot be classified into particular band alignments due to the very strong modifications to the band structure caused by the large lattice mismatch between nitrides and non-nitrides. Many interesting structures involve antimonides and it is fortunate that antimonide-containing wires can also be grown in heterostructures.[20] It is important to realize that the same materials combination can have different band alignments depending on segment thickness and the wire orientation may also play a role. We give figures for the band structure of short segments, which are equivalent to strained layers, allowing easy identification of, for example, interesting band gaps.

A. Type I-s

Type I-s structures are maybe the most conventional, where the segment is a quantum well, between barriers formed by the wire material. Figure 4 shows a typical ex-

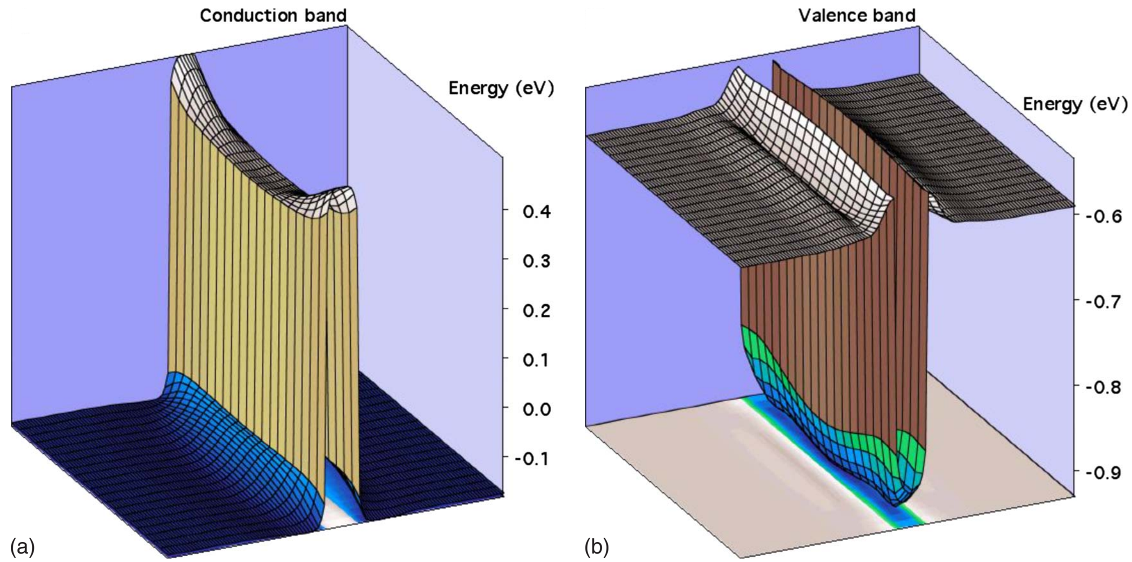

FIG. 6. (Color online) (a) A surface plot of the conduction-band minimum for a [001] oriented wire defined in Fig. 1(a) consisting of an InAs wire with an InP segment. The length of the InP segment is 50 and the width of the wire is 100. (b) A surface plot of the valence-band maximum for the same wire.

ample. These structures are often used in light emitting devices such as lasers, where it is advantageous if the band gap in the well is direct. There is a large amount of work being done to make homogeneous and segmented wires into efficient light emitting devices. The materials combinations that give type I-s structures are (GaN, InN)/AlN, InN/GaN, (AlAs, InP, InAs, AlSb, GaSb, InSb)/AlP, (GaAs, InP, InAs, AlSb, GaSb, InSb)/GaP, (GaAs, InP, InAs, AlSb, GaSb, InSb)/AlAs, (AlP, InAs, GaSb, InSb)/GaAs, (GaAs, InAs, InSb)/InP, (GaAs, GaSb, InSb)/AlSb, InSb/GaSb, and AlP/InSb. The materials before the slash are in the segment and the material after the slash forms the barrier. In our calculations we find that InAs in GaAs can be made to emit at a wavelength of 1.55 μm, which is technically important. InSb can either be type I-s or have a negative band gap if grown between barriers of InP. Consequently arbitrarily low band gaps (albeit indirect) can be obtained in this system. A

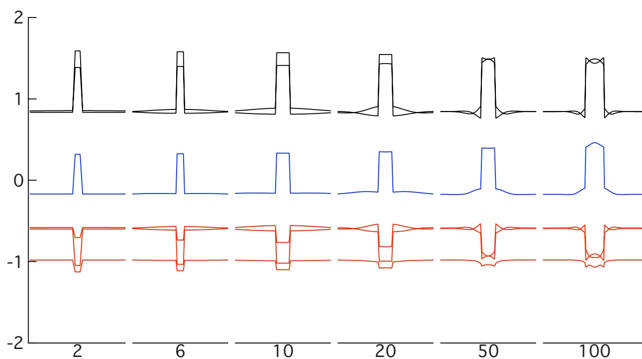

FIG. 7. (Color online) The band edges in a [001] oriented wire consisting of InAs with an InP segment. The plots are along the center of the wire. The length of the InP segment was varied from 2 to 100, where the width of the wire (along the x direction) was 100. The blue trace is the Γ conduction band, black traces are the X conduction bands, and red traces are the valence bands.

quantum well with a high band gap is GaN in AlN, which has a band gap of 3.5 eV and still has barrier heights of about 0.5 eV for both electrons and holes, giving the possibility of strong confinement. InN in AlN has barrier heights of several eV which might allow high-temperature operation of lasers based on quantum wells in these wires.

B. Type I-b

In type I-b structures the segment forms a barrier for both electrons and holes. Figure 7 shows a typical example. The material combinations giving type I-b structures are AlN/GaN, (AlN, GaN)/InN, (GaP, AlAs)/GaAs, (AlP, GaP, AlAs)/InP, (AlP, GaP, AlAs, GaAs, InP)/InAs, (GaP, AlAs, AlSb)/GaSb, and (AlP, AlAs, InP, AlSb, GaSb)/InSb. These structures may thus be of use in tunneling devices, which has been demonstrated, for example, in InP/InAs nanowires.[21] InP/InAs has a predicted direct gap barrier height of about 0.5 eV for electrons, in fair agreement with somewhat indirect measurements.[2] The barrier is smaller for holes.

C. Type II-s

In type II-s structures the segment forms a well for electrons and a barrier for holes. The material combinations giving type II-s structures are (AlP, AlAs)/GaP, AlP/GaAs, AlP/AlAs, (AlP, InP)/GaAs, (AlP, GaP, AlAs, GaAs, InP, InAs)/AlSb, and (AlP, GaP, GaAs, InP)/GaSb. These structures may be of use in devices based on hole tunneling. Furthermore, if the wire is excited with light having an energy larger than the band gap, electron-hole pairs will be created. They will separate spontaneously, electrons to the segment and holes to the barrier, until equilibrium is established. When the situation is in equilibrium we have a gas of electrons adjacent to a gas of holes, which will be discussed in Sec. V. In Fig. 11 we show the band structure of InP/GaAs wires. For long segments the structure is type II-s, but for short

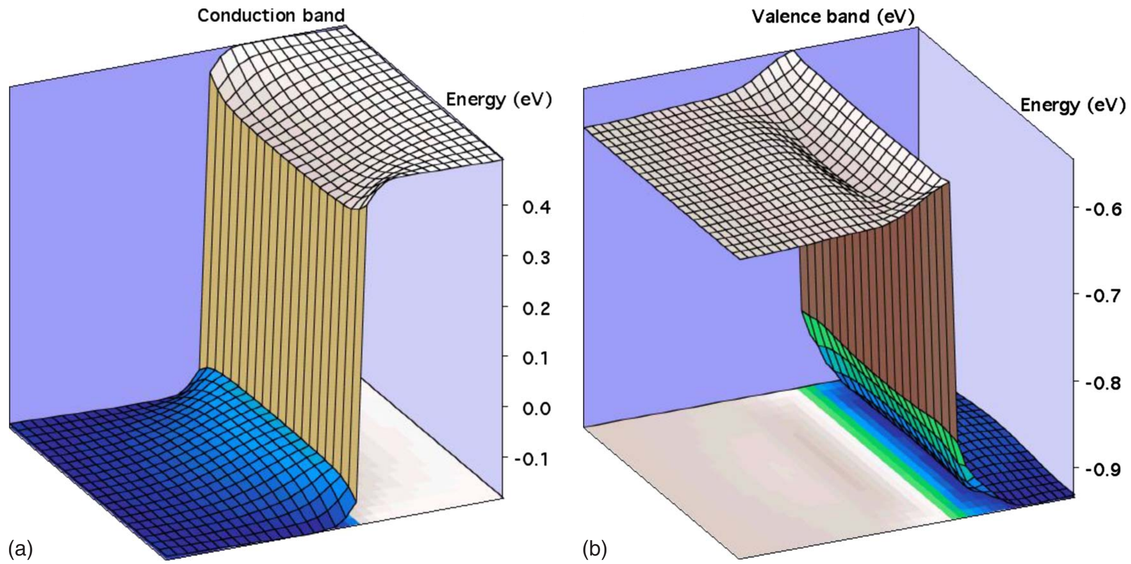

FIG. 8. (Color online) Surface plots of the band edges in a wire consisting of a heterostructure of InAs and InP. The wire is oriented along the [001] direction. InAs is to the left of the interface.

segments we find that the InP is a barrier for both electrons and holes. GaP/AlSb is calculated to have a hole barrier of close to 1 eV for quite wide segments, although the electron well is quite shallow. AlP/GaP is more symmetric having barriers of about 300 meV for holes and forming a quantum well with about the same barriers for electrons. This is thus a good system for creating dipolar bilayers, although it will be necessary to cap the AlP segment to avoid decomposition by humid air.

D. Type II-b

In type II-b structures the segment forms a barrier for electrons and a well for holes. The material combinations giving type II-b alignments are (GaP, AlAs, GaAs, InP, AlSb, GaSb)/AlP, (GaP, AlSb)/AlAs, (AlSb, GaSb)/GaAs, (GaP, GaAs, AlSb, GaSb)/InP, and (GaAs, AlSb)/InAs. These structures may be of use in devices based on electron tunneling. Often it is better to use electrons as the active charge carrier in tunneling devices rather than holes because of their lower effective mass. Similarly to the type II-s structures we can create a gas of dipoles in the wires.

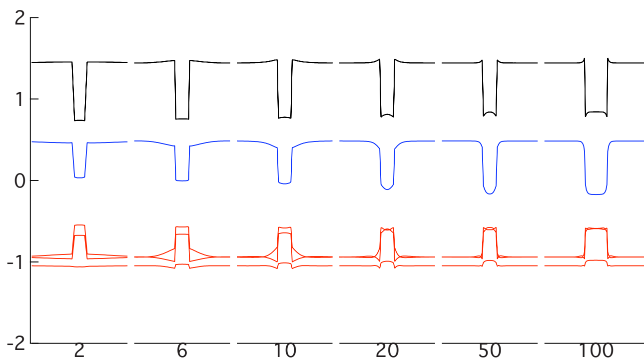

FIG. 9. (Color online) The band edges in a [111] oriented InP wire with an InAs segment. The plot is through the center of the wire. The length of the InAs segment was varied from 2 to 100, where the width of the wire (along the x direction) was 100. The blue trace is the Γ conduction band, black traces are the X conduction bands, and red traces are the valence bands.

E. Type III-s

In type III-s structures the conduction-band minimum of the segment is below the valence-band maximum of the barrier. The material combinations giving type III-s alignments are InAs/GaSb, (GaP, InP, InAs, GaSb)/InSb. In these structures we have a spontaneous charge separation, where electrons will transfer from the top of the valence band in the barrier into the conduction band of the segment, leaving

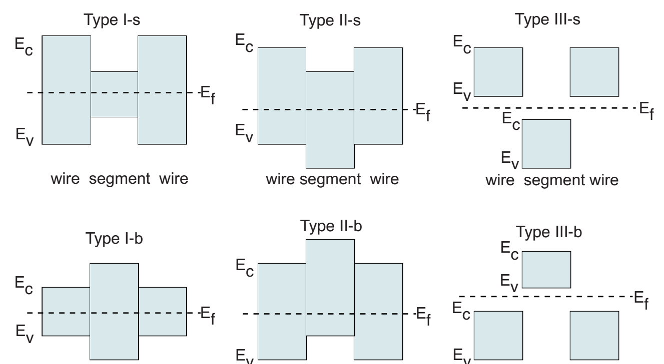

FIG. 10. (Color online) Different band offsets that may occur at a segment. The letters s (for segment) or b (for barrier) indicate which material has the lowest energy conduction-band minimum. Type I-s is a normal quantum well, confining both electrons and holes to the segment. Type II-s confines electrons to the segment and holes to the wire or barrier. Type III-s is metallic and the conduction-band minimum of the segment is below the valence-band maximum of the barrier, giving rise to transfer of electrons to the segment and holes to the barrier. The inverted structures may also occur denoted by type I-b, type II-b, and type III-b.

TABLE II. Band alignments in different segmented wires when the wire is grown in the [100] direction. The notation of the alignment is explained in Fig. 10. We have also indicated whether the lowest conduction band is direct (labeled "dir") or indirect (labeled "ind"). met-s or met-b indicates that the structure has a negative gap in the segment or barrier, respectively. The notation follows the thickness of the segments, i.e., "II-s, I-b" means that the band alignment is type II-s for short segments and type I-b for long segments.

	Segment material								
Barrier material	AlP	GaP	AlAs	GaAs	InP	InAs	AlSb	GaSb	InSb
AlP		II-b ind	I-s, II-b ind	II-b ind	II-b, I-s ind, dir	I-s dir	I-s, II-b ind	I-s, II-b ind	met-s, I-s ind
GaP	II-s ind		II-s ind	I-s ind, dir	I-s dir	I-s dir	I-s ind	I-s ind	met-s, I-s ind
AlAs	II-s ind	II-b ind		I-s dir	I-s dir	I-s dir	I-s, II-b ind	I-s ind	met-s, I-s ind
GaAs	II-s, I-b ind, dir	I-b dir	I-b dir		II-s dir	I-s dir	II-b dir	I-s, II-b ind, dir	met-s, I-s ind
InP	I-b dir	II-b, I-b dir	I-b dir	I-s, II-b dir		I-s dir	II-b dir	II-b dir	met-s, I-s dir
InAs	I-b dir	I-b dir	I-b dir	II-b, I-b dir	I-b dir		II-b dir	III-b dir	III-b dir
AlSb	II-s ind	II-s dir	II-s ind	I-s, II-s dir	II-s dir	II-s dir		I-s dir	I-s ind, dir
GaSb	II-s ind	II-s, I-b dir	I-b dir	II-s dir	II-s dir	III-s dir	I-b dir		I-s ind, dir
InSb	I-s, I-b, met-b ind, dir	III-s, met-b dir	I-b, met-b dir	met-s, met-b dir	III-s dir	met-s, III-s dir	I-b dir	III-s, I-b dir	

TABLE III. Band alignments in different segmented wires when the wire is grown in the [111] direction. The notation is the same as in Table II.

	Segment material								
Barrier material	AlP	GaP	AlAs	GaAs	InP	InAs	AlSb	GaSb	InSb
AlP		II-b ind	I-s, II-b ind	II-b, I-s ind, dir	II-b, I-s ind, dir	I-s dir	I-s, II-b ind	I-s, II-b ind	met-s, I-s dir
GaP	II-s ind		II-s ind	I-s ind, dir	I-s dir	I-s ind	I-s, II-b ind	I-s ind, dir	met-s, I-s ind, dir
AlAs	I-b, II-s ind	II-b ind		I-s dir	I-s dir	I-s dir	I-s, II-b ind	I-s ind, dir	met-s, I-s dir
GaAs	I-b dir	I-b dir	I-b dir		I-b, II-s dir	I-s dir	II-b dir	II-b dir	met-s, I-s dir
InP	I-b dir	II-b, I-b dir	I-b dir	I-s, II-b dir		I-s dir	II-b dir	II-b dir	met-s, I-s dir
InAs	I-b dir	I-b dir	I-b dir	II-b, I-b dir	I-b dir		II-b dir	III-b dir	III-b dir
AlSb	II-s dir, ind	I-s, II-s dir, ind	II-s dir, ind	I-s, II-s dir	II-s dir	II-s dir		I-s dir	I-s ind, dir
GaSb	I-b dir	II-s, I-b dir	I-b dir	II-s dir	II-s dir	III-s dir	I-b dir		I-s ind, dir
InSb	I-b, met-b, I-b dir	III-s, met-b, I-b dir	I-b, I-s dir	met-s, III-s, I-b dir	III-s, I-b dir	met-s, III-s dir	I-b dir	I-s, I-b dir	

TABLE IV. Band alignments in different segmented nitride-based wires, which is independent of the growth direction of the wire. The notation is the same as in Table II.

	Segment material		
Barrier material	AlN	GaN	InN
AlN		I-s, dir	I-s, dir
GaN	I-b, dir		I-s, dir
InN	I-b, dir	I-b, dir	

holes behind. In Fig. 12 we show the band structure of InAs/InSb wires grown along the [111] direction. This materials combination is unusually interesting. For short segments the InAs has a negative band gap and is thus metallic. For longer segments the structure is type III-s, which is metallic by charge transfer. It is thus possible to make the InAs into a metal in two different ways simply by tuning the length of the segment. Such wires have been fabricated.[22]

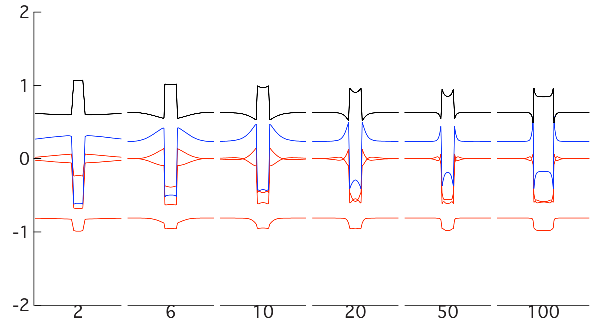

FIG. 12. (Color online) The band structure of [111] oriented wires consisting of an InAs segment in InSb. For short segments we have a negative band gap in the InAs. For longer segments the InAs conduction-band minimum is below the valence-band maximum of the InSb. As a result electrons will accumulate in the InAs segment and holes in the InSb barrier. The blue trace is the Γ conduction band, black traces are the *X* conduction bands, and red traces are the valence bands.

F. Type III-b

In type III-b structures the conduction-band minimum of the barrier is below the valence-band maximum of the segment. The material combinations with III-b alignments are (GaSb, InSb)/InAs. In these structures we again have spontaneous charge separation where holes will accumulate in the segment leaving electrons in the barrier. We have the opportunity to have a stable hole gas in a confined volume, which is interesting. Figure 13 shows the band structure of InSb/InAs wires. The wire is oriented along the [111] direction. For all segment lengths the structure is type III-b. These systems have been proposed as a means to manipulate electron spins.

G. Negative band gaps

InSb wires with segments of GaAs or InAs have negative band gaps in the segments. The segments are then metallic. It is also possible to have a metallic barrier close to the segment in the case of (AlP, GaP, AlAs, GaAs)/InSb. This situation is quite remarkable since it is then possible to have a wire with a homogeneous stoichiometry that starts out as a metal close to the segment interface and then transforms to a semiconductor further away from the interface. This certainly should be regarded as a metal-semiconductor transition without disturbance from interface defects. The systems InSb/(AlP, GaP, AlAs, GaAs, InP) involve metallic segments of InSb.

Figures 14–16 summarize the band structures that occur for short segments which behave like two-dimensional strained layers. Since long segments have the same band structure as the bulk material it is possible to estimate the band structure for intermediate length segments using these figures. The figures on the website give a fuller picture.[11] Reference 33 gives the effective masses for many of these quantum well systems, along with a graph for estimating the confinement energy.

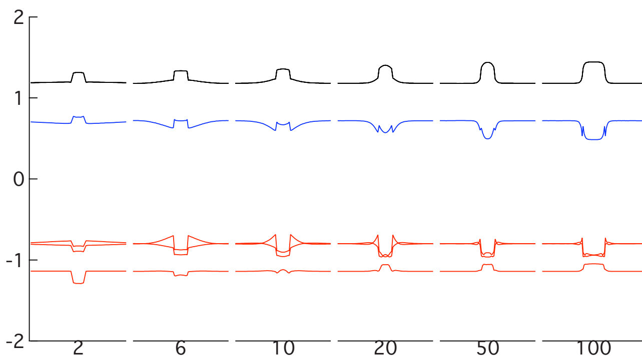

FIG. 11. (Color online) The band structure of [111] oriented wires consisting of an InP segment in GaAs. Blue trace is the Γ conduction band, black traces are the *X* conduction bands, and red traces are the valence bands.

V. APPLICATIONS IN SCIENCE AND TECHNOLOGY

There are applications in science for which segmented wires are more suited than strained layers and quantum dots. In some cases this is due to the greater flexibility in materials

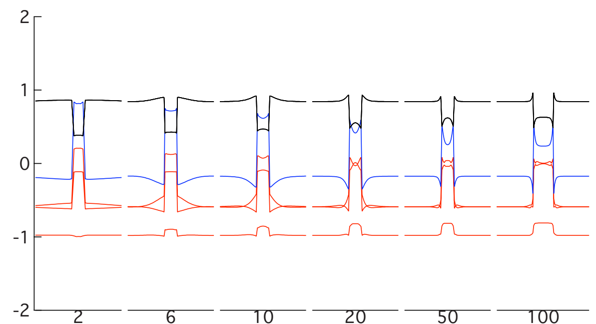

FIG. 13. (Color online) The band structure of [111] oriented wires consisting of an InSb segment in InAs. The blue trace is the Γ conduction band, black traces are the *X* conduction bands, and red traces are the valence bands.

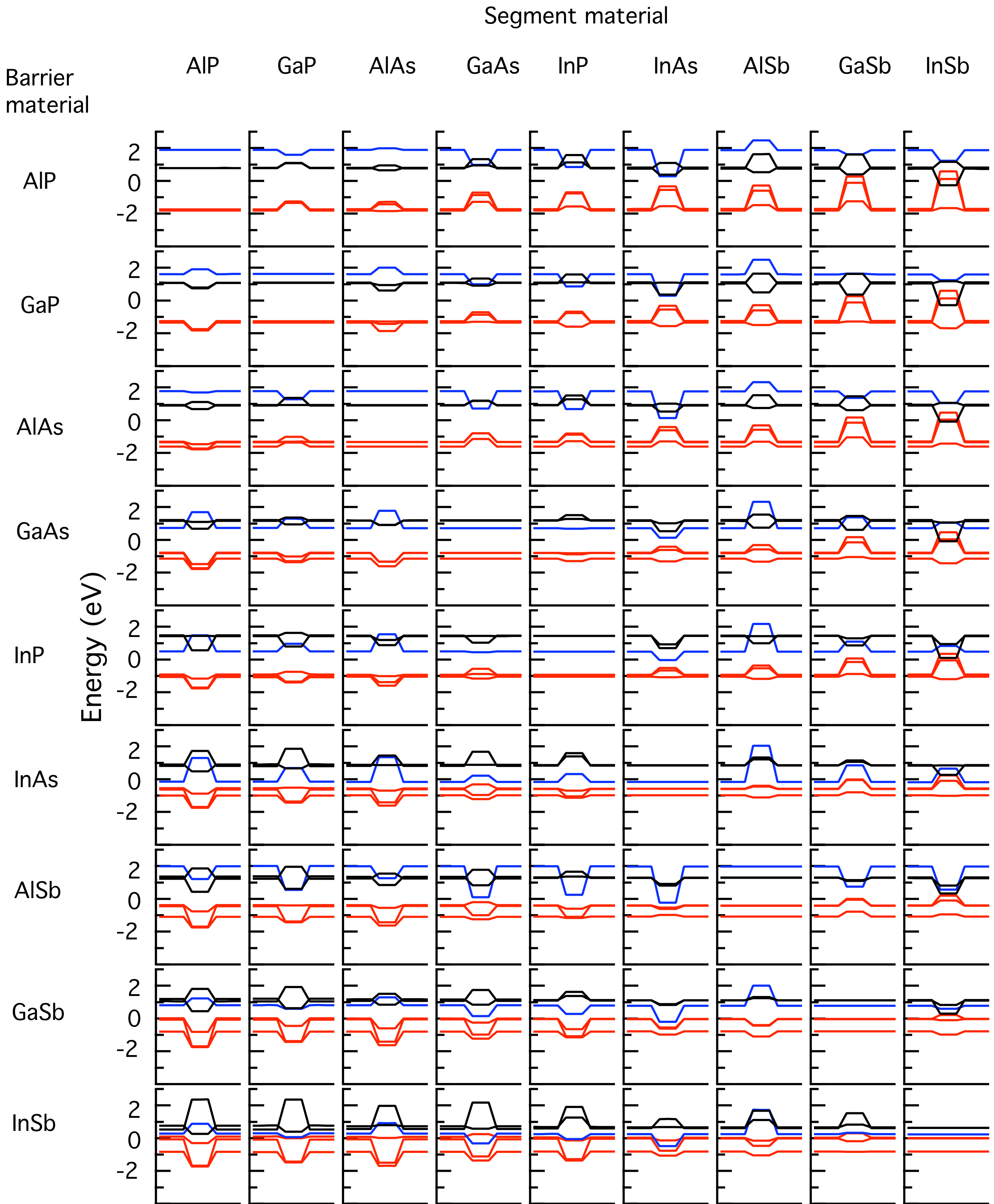

FIG. 14. (Color online) Overview of the band structure of segmented wires oriented along the [001] direction where the segment length is 2 and the wire width is 100. Such short segments behave like strained two-dimensional layers. The blue trace is the Γ conduction band, black traces are the X conduction bands, and red traces are the valence bands.

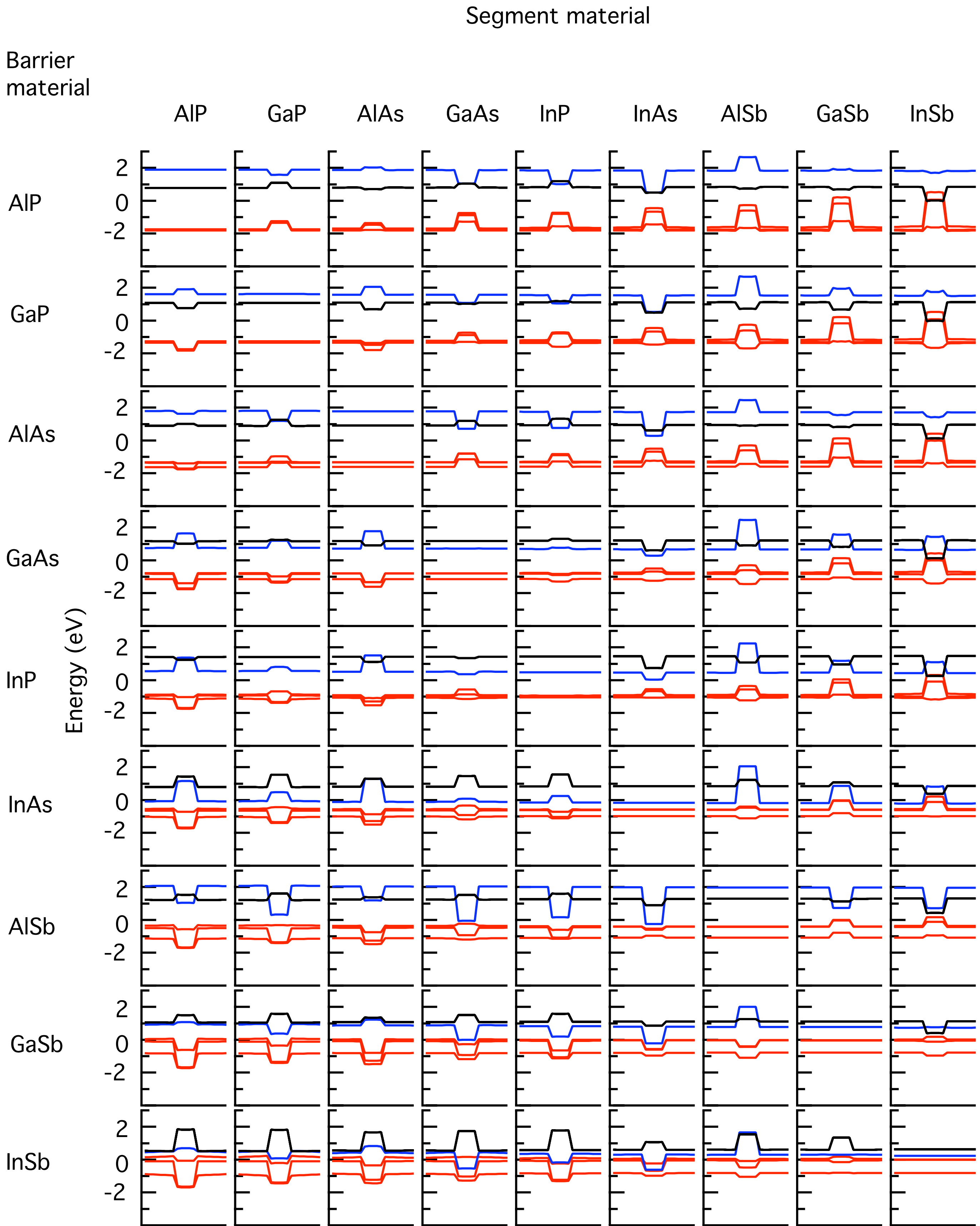

FIG. 15. (Color online) Overview of the band structure of segmented wires oriented along the [111] direction where the segment length is 2 and the wire width is 100. Such short segments behave like strained two-dimensional layers. The blue trace is the Γ conduction band, black traces are the X conduction bands, and red traces are the valence bands.

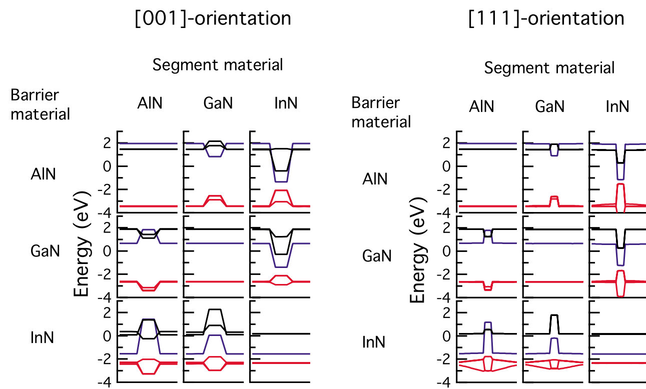

FIG. 16. (Color online) Overview of the band structure of segmented nitride wires, where the segment length is 2 and the wire width is 100. Such short segments behave like strained two-dimensional layers. Blue trace is the Γ conduction band, black traces are the X conduction bands, and red traces are the valence bands.

combinations that wires allow compared with the other systems. In other cases the lateral confinement can be used to an advantage. The precise control over segment position that can be obtained in wires can be used to tune interesting properties. We will in this section describe a few applications using segmented wires in science and technology that we hope will inspire experimental work. This includes some approaches to the notoriously difficult problem of obtaining Ohmic contacts to nanowires.

A. Exotic dipole phases

There are many wire systems that are interesting from a basic physics point of view. The type II and type III systems will allow the creation of exciton gases which are polarized, as illustrated in Fig. 17. This is often called a dipole gas and in our case it will be a gas of aligned dipoles. In the type II systems the concentration (or equivalently r_s which measures the interparticle distance) of the dipole gas can be externally tuned by an exciting laser. In the type III system no laser is needed since the dipole gas is the ground state. Due to Coulomb repulsion between the excitons or dipoles there is a strong tendency for correlation between the dipoles. There are several theoretical studies predicting that dipolar layers have rich physics involving interesting phases such as dipole liquids, dipole solids, Coulomb liquids, Coulomb solids, and Wigner supersolids.[23,24] The dipole liquid is a superfluid. Most of these phases have not been observed experimentally. The advantage of using wires instead of layers with a type II band alignment is that the dipole gas is confined in the transverse direction so that the dipoles cannot diffuse away, allowing the creation of a high-density dipolar gas. Another advantage is that the distance between the electron and hole layers can be tuned during growth. It is known that the electron-hole separation is a very important parameter in the phase diagram of dipolar systems. Furthermore it is possible to couple several dipole layers and such coupled dipolar layers should have their own very interesting elementary excitations, very likely at low energies.

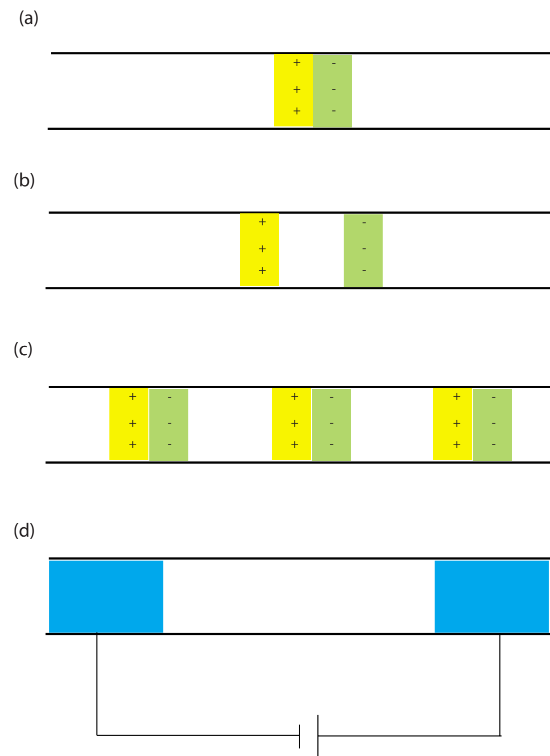

FIG. 17. (Color online) (a) A drawing of a dipole gas in a wire. (b) It is possible to separate the electron and hole gases by using a spacer layer. (c) Periodic arrays of dipole gases can be contemplated. (d) Schematic of electrically contacting a wire device using negative gap semiconductors for the contacting regions.

B. Transport physics

Type III-b structures are interesting for transport studies. We have the curious situation that under applied bias, electrons will carry the current in the barriers but inside the segment the current is passed by holes, given suitable doping. Effects arising from the change in sign of the effective mass when passing the barrier should be interesting to study, in particular for superlattice studies where there are cases where only the mass is modulated. Effective mass superlattices are an old idea of Sasaki.[25] We here view the difference between electrons and holes as merely being having different signs for the effective mass. Holes experience strong spin-orbit interaction in the segment which might be used to manipulate the spin of the electrons.[26] One idea is to inject electrons into the segment, manipulate the spin of the hole using an external electric field, and to collect the spin-manipulated electrons at the collector.

C. Contacting technology

It is usually very difficult to make reliable Ohmic and Schottky contacts to semiconductors[27] such as nanowires using normal technologies, such as depositing a suitable metal on the wire. This is due to poor surface quality of the semiconductor and the fact that the metal is never epitaxial to the wire. By using segments that are metallic it may be possible to alleviate this problem since metal-metal contacts are much

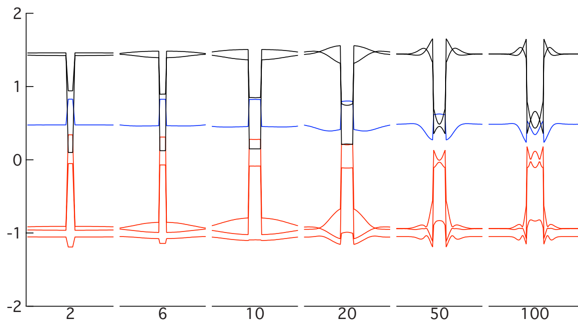

FIG. 18. (Color online) Band structure of [001] oriented wires consisting of a segment of InSb in InP. Short segments have a negative band gap with a Fermi level close to the conduction band of InP, assuming that the Fermi level is between the valence-band maximum and the conduction-band minimum. Blue trace is the Γ conduction band, black traces are the *X* conduction bands, and red traces are the valence bands.

more forgiving than metal-semiconductor contacts, with respect to contact resistance. Figure 17 shows a basic illustration how this could be done. The contacting segments could have a negative gap and this segment could have the Fermi level close to the conduction or valence band of the semiconducting wire giving an Ohmic contact. Alternatively the segment may have the Fermi level in the middle of the gap of the semiconducting wire, giving a Schottky type of contact with a diode-type behavior. For example, a thin InSb segment in InP has a negative gap and is calculated to have the Fermi level close to the conduction-band minimum of InP, thus giving an Ohmic contact to *n*-type InP. The band structure for this system is given in Fig. 18, with a wire oriented along the [001] direction. We also predict a negative gap if the wire is oriented along the [111] direction. We also find that a thin InSb segment should give an Ohmic contact to *n*-type GaAs although the Fermi level of the InSb is a bit deeper than when InSb is a segment in InP. For InSb in GaP we predict metallic InSb where the Fermi level of InSb is in the middle of the band gap of GaP, thus giving a Schottky type of junction. There are no non-nitride segments with a negative gap and a Fermi level close to the valence band of the technically important wire materials InP and GaAs.

D. Plasmonics

The metallic systems will be plasmonically active, if they have a negative gap or are metallic due to the presence of a dipole gas system. Since it is possible to fabricate the wires very precisely it will be possible to tune the separation of the plasmonically active segments allowing very reproducible coupling between them. This is advantageous if, for example, the wires are to be used to enhance Raman scattering.[28] Usually surface enhanced Raman scattering suffers from the random placement of metal particles on a surface and most particles do not form a pair with the appropriate distance between them.

E. Strain engineering

Due to their limited cross section, nanowires allow heterojunctions that are not stable in large planar structures. For example, InSb has a negative gap close to the interface of GaAs but becomes semiconducting away from the interface where the strain is less. We thus have a continuous transition from a metal to a semiconductor within the same material. Finally we would like to mention a possibility which is quite unique for segmented nanowires. Since the segments are allowed to relax as well as to strain the barrier, when grown on a barrier of a different lattice constant, it is possible to grow segmented wires with a large lattice mismatch between the segment and the barrier.[29] This is especially true for narrow wires. Suppose we have a segment in compression. By capping the segmented wire with the barrier material the compression will increase and there is a possibility that the segment (now a dot) will undergo a phase transition to a new crystal structure. Phase transitions in III-V semiconductors typically occur at a hydrostatic pressure of a few hundred kbar[30] which can easily be obtained in the more highly strained systems. External hydrostatic pressure has previously been shown to cause phase transitions in quantum wells.[31] This fairly simple method also allows the study of materials under higher hydrostatic *tension* than can be obtained in strained layers. We note that Stranski-Krastanow dots never form if they are under tension.[32]

VI. SUMMARY

By computing the band structure of all combinations of AlN, GaN, InN, AlP, GaP, AlAs, GaAs, InP, InAs, AlSb, GaSb, and InSb where one compound is a segment in the other, we have identified a large set of interesting structures. These structures include metallic segments and segments which support dipole gases. All combinations have been classified with respect to band alignment, except nitride non-nitride combinations which behave too wildly to be classifiable. Using this information it is also possible to verify that certain combinations of, e.g., band gap and band alignment do not occur among the investigated material combinations.

ACKNOWLEDGMENTS

We acknowledge F. Boxberg for interesting discussions and independent confirmation of some of the strain results using a separate computer program. We thank U. Håkanson, S. Gray, and N. Anttu for a critical reading of the paper. This work was performed within the Nanometer Structure Consortium in Lund and supported by the Swedish Foundation for Strategic Research (SSF) and the Swedish Research Council (VR).

*mats-erik.pistol@ftf.lth.se
†craig-pryor@uiowa.edu

[1] K. A. Dick, Prog. Cryst. Growth Charact. Mater. **54**, 138 (2008).
[2] M. T. Björk, B. J. Ohlsson, T. Sass, A. I. Persson, C. Thelander, M. H. Magnusson, K. Deppert, L. R. Wallenberg, and L. Samuelson, Appl. Phys. Lett. **80**, 1058 (2002).
[3] N. Sköld, L. S. Karlsson, M. W. Larsson, M.-E. Pistol, W. Seifert, J. Trägårdh, and L. Samuelson, Nano Lett. **5**, 1943 (2005).
[4] Z. Zanolli, L.-E. Fröberg, M. T. Björk, M.-E. Pistol, and L. Samuelson, Thin Solid Films **515**, 793 (2006).
[5] D. Appell, Nature (London) **419**, 553 (2002).
[6] L. J. Lauhon, M. S. Gudiksen, and C. M. Lieber, Philos. Trans. R. Soc. London, Ser. A **362**, 1247 (2004).
[7] H. Sakaki, Jpn. J. Appl. Phys. **19**, L735 (1980).
[8] L. C. L. Y. Voon, Y. Zhang, B. Lassen, M. Willatzen, Q. Xiong, and P. C. Eklund, J. Nanosci. Nanotechnol. **8**, 1 (2008).
[9] M. E. Pistol and C. E. Pryor, Phys. Rev. B **78**, 115319 (2008).
[10] X. Duan and C. M. Lieber, Adv. Mater. **12**, 298 (2000).
[11] http://semiconductor.physics.uiowa.edu/Slices/Supplementary.html
[12] See EPAPS Document No. E-PRBMDO-80-052927 for numerical data for the band structure of our calculated materials combinations. For more information on EPAPS, see http://www.aip.org/pubservs/epaps.html.
[13] M. C. Muñoz and G. Armelles, Phys. Rev. B **48**, 2839 (1993).
[14] W. J. Fan, M. F. Li, T. C. Chong, and J. B. Xia, J. Appl. Phys. **79**, 188 (1996).
[15] L. Landau and E. Lifshitz, *Elasticity* (Pergamon, London, 1959).
[16] T. B. Bahder, Phys. Rev. B **41**, 11992 (1990).
[17] I. Vurgaftman, J. R. Meyer, and L. R. Ram-Mohan, J. Appl. Phys. **89**, 5815 (2001).
[18] I. Vurgaftman and J. R. Meyer, J. Appl. Phys. **94**, 3675 (2003).
[19] S. I. Rybchenko, R. Gupta, K. T. Lai, I. E. Itskevich, S. K. Haywood, V. Tasco, N. Deguffroy, A. N. Baranov, and E. Tournié, Phys. Rev. B **76**, 193309 (2007).
[20] Y. N. Guo, J. Zou, M. Paladugu, H. Wang, Q. Gao, H. H. Tan, and C. Jagadish, Appl. Phys. Lett. **89**, 231917 (2006).
[21] M. T. Björk, B. J. Ohlsson, C. Thelander, A. I. Persson, K. Deppert, L. R. Wallenberg, and L. Samuelson, Appl. Phys. Lett. **81**, 4458 (2002).
[22] P. Caroff, J. B. Wagner, K. A. Dick, H. A. Nilsson, M. Jeppsson, K. Deppert, L. Samuelson, L. R. Wallenberg, and L.-E. Wernersson, Small **4**, 878 (2008).
[23] P. Hartmann, Z. Donko, and G. Kalman, Europhys. Lett. **72**, 396 (2005).
[24] Y. N. Joglekar, A. V. Balatsky, and S. Das Sarma, Phys. Rev. B **74**, 233302 (2006).
[25] A. Sasaki, Phys. Rev. B **30**, 7016 (1984).
[26] V. Sih and D. D. Awschalom, J. Appl. Phys. **101**, 081710 (2007).
[27] R. T. Tung, Phys. Rev. B **45**, 13509 (1992).
[28] S. Nie and S. R. Emory, Science **275**, 1102 (1997).
[29] F. Glas, Phys. Rev. B **74**, 121302(R) (2006).
[30] R. K. Singh and S. Singh, Phys. Rev. B **39**, 671 (1989).
[31] B. A. Weinstein, S. K. Hark, R. D. Burnham, and R. M. Martin, Phys. Rev. Lett. **58**, 781 (1987).
[32] W. Seifert, N. Carlsson, M. Miller, M. Pistol, L. Samuelson, and L. Wallenberg, Prog. Cryst. Growth Charact. Mater. **33**, 423 (1996).
[33] C. Pryor and M.-E. Pistol, Phys. Rev. B **72**, 205311 (2005).